Quaternary Science Reviews 325 (2024) 108498

Contents lists available at ScienceDirect

Quaternary Science Reviews

journal homepage: www.elsevier.com/locate/quascirev

Separation of the Asian summer monsoon and local precipitation from stalagmite oxygen isotope records in Eastern China during the last millennium

Zunyu Hu[a], Haowen Fan[a,**], Yuhui Liu[b], Zhipeng Wu[c], Chaoyong Hu[a,b,*]

[a] School of Geography and Information Engineering, China University of Geosciences, Wuhan, 430074, China
[b] State Key Laboratory of Biogeology and Environmental Geology, China University of Geosciences, Wuhan, 430074, China
[c] Earth and Climate Research Center, Earth and Life Institute, Université Catholique de Louvain, Louvain-la-Neuve, 1348, Belgium

A R T I C L E I N F O

Handling Editor: Mira Matthews

Keywords:
Asian summer monsoon
Precipitation reconstruction
Stalagmite oxygen isotope
Last millennium
Eastern China

A B S T R A C T

The Asian summer monsoon (ASM) regulates water vapor and heat transport across the East Asian continent and has a significant impact on patterns of regional precipitation. However, assessment of the long-term association between the monsoon and precipitation in different regions remains difficult due to spatial chronological differences and uncertainties in interpretation of climate proxies. This study provides a novel insight into the interpretation of stalagmite oxygen isotopes ($\delta^{18}O$) records and obtained synchronous ASM index series and precipitation variations in Northern China (NC), Central China (CC), and Southwestern China (SWC) over the last 1134 years (850–1983CE). The results show that the ASM index sequence is consistent with the trend evident in the monsoon intensity records from the region upstream of the water vapor source, which represents the response to the inter-hemispheric temperature dominated by effective solar radiation (ESR). Reconstruction precipitation data were in general agreement with the existing paleo-hydrological records of the regions, confirming the reliability and chronological accuracy of the reconstruction. Correlation analysis highlighted the significant regional heterogeneity in the destabilizing relationship between precipitation and the monsoon over the past millennium in Eastern China at sub-centennial scales. Specifically, the precipitation-monsoon relationships in three regions, NC, CC, and SWC, might be related to the North Atlantic Oscillation (NAO), the position of the intertropical convergence zone (ITCZ), and solar activity, respectively. Moreover, at the millennial scale, a certain positive correlation between precipitation and ASM in NC and SWC was identified, whereas there was a weaker correlation between precipitation and ASM in CC. This study represents an attempt to further interpret the stalagmite $\delta^{18}O$ record, which can be generalized to larger and longer time scales.

1. Introduction

The Asian summer monsoon (ASM) regulates the transport of water vapor and heat across the East Asian continent and it is closely linked to the global climate system in different regions through atmospheric circulation and ocean-atmosphere coupling (Ding and Chan, 2005). Most monitoring has indicated that rainfall over the summer monsoon contributes 40%–50% (and 60%–70%) of total annual precipitation in southern (and northern) regions of China, respectively. Therefore, in addition to posing a threat to the lives and property of the large human population in the region, monsoonal activity is of enormous significance for regional and local water resources (Zhou et al., 2009). During the second half of the last century, the ASM experienced rapid weakening, while precipitation in Eastern China transitioned from a "positive-negative-positive" meridional triple pattern to a "southern flooding-northern drought" pattern (Ding et al., 2008; Zhou et al., 2009). Previous studies have shown that the distribution of drought and flood in Eastern China is related to the movements of rain belts, which are regulated by the ASM and climate modes (Ding et al., 2008, 2009; Wang et al., 2020; Xue et al., 2023). This implies that any disturbance of the normal advance or retreat of the monsoon rain belt regulated by the ASM under different atmospheric circulation backgrounds can result in either deficient or excessive precipitation (Shekhar et al., 2022; Zhao et al., 2020). However, previous studies have shown that the

* Corresponding author. School of Geography and Information Engineering, China University of Geosciences, Wuhan, 430074, China.
** Corresponding author. School of Geography and Information Engineering, China University of Geosciences, Wuhan, 430074, China.
E-mail addresses: fanhaowen@cug.edu.cn (H. Fan), chyhu@cug.edu.cn (C. Hu).

https://doi.org/10.1016/j.quascirev.2023.108498
Received 7 October 2023; Received in revised form 28 December 2023; Accepted 28 December 2023
Available online 4 January 2024
0277-3791/

relationships between ASM and precipitation (ASM - precipitation relationship) in Eastern China might have destabilized over the last few decades, possibly due to internal variability (Li et al., 2010; Sun et al., 2017). Since it is predicted that atmospheric circulation will change dramatically under different future emission scenarios (Cai et al., 2022), there is an urgent need to understand variations in the ASM and precipitation in Eastern China under the various climatic backgrounds and their relationships.

The Medieval Climate Anomaly (MCA; 900–1300 CE) and the Little Ice Age (LIA; 1350–1850 CE) represent two important climatic stages that have occurred under different temperature and circulation conditions over the last millennium. Some studies have pointed to a general "dry southern and wet northern" pattern during the MCA in Eastern China, but a "wet southern and dry northern" pattern during the LIA (Chen et al., 2015; Jiang et al., 2023; Wang et al., 2022). In addition, the precipitation distribution is closely related to different atmospheric circulation variabilities. Thus, MCA/LIA allows the study of the response of precipitation to ASM under different atmospheric circulation backgrounds. Many previous paleo-climatic studies have observed evidently stable coupling ASM-precipitation relationships in different regions over Eastern China during the last millennium (Jiang et al., 2023; Tan et al., 2018; Zhang et al., 2008). Several studies also reconstructed local palaeohydrological changes based on this stable ASM-precipitation relationship (Yang et al., 2021; Zhang et al., 2008). However, a previous modeling study found that the stability of the ASM - precipitation relationship is applicable at only centennial and longer time scales, whereas the relationship is unstable at shorter time scales, possibly due to the internal variability of the climate system (Shi et al., 2018). A deeper understanding of the ASM-precipitation relationship in different regions requires reliable ASM records as well as cross-regional paleo-precipitation reconstructions. Some paleo-hydrological networks based on the multiple paleoclimatic proxies were used to investigate the precipitation distributions in Eastern China during the MCA/LIA period (e.g. Chen et al., 2015; Hao et al., 2023; Shi et al., 2019). However, inter-regional paleo-precipitation variability and its sub-centennial scale relationships with the ASM remain unclear due to record differences in temporal resolution, chronology, and proxy sensitivity to hydroclimate among different paleo-climate archives. The examination of the relationship between the monsoon and precipitation based on evidence from the same paleoclimatic material may be an innovative solution that avoids the above-mentioned uncertainties as far as possible.

Cave stalagmites have been extensively used in paleoclimate studies over the past several decades. Stalagmite records have allowed high resolution and accurate dating within reconstructions of paleoclimate variations since the late Pleistocene, which are helpful for a deeper understanding of the evolution of Earth's climate system (Cheng et al., 2016). The carbonate oxygen isotope ($\delta^{18}O$) is a proxy most widely used in stalagmite paleoclimate studies. However, since stalagmite $\delta^{18}O$ is influenced by both hydrology and atmospheric circulation over multiple processes, both these factors need to be considered in paleoclimate reconstruction (Wang et al., 2022). For example, increased local and regional rainfall may lead to stronger Rayleigh distillation and weaker evapotranspiration effects, respectively, whereas decreased local and regional rainfall have the opposite effect, e.g., "amount effect". Though several published studies have reconstructed local paleo-precipitation using stalagmite $\delta^{18}O$ records from caves based on the negative correlation between stalagmite $\delta^{18}O$ and local monitored precipitation (Tan et al., 2009; Zhang et al., 2008; Zhao et al., 2020), the uncertainties in the association between $\delta^{18}O$ and local precipitation have increased with increasing number of related studies, which show a significant correlation between upstream precipitation/atmospheric circulation and the stalagmite $\delta^{18}O$ record (Baker et al., 2015; Cai et al., 2017; Pausata et al., 2011; Tan, 2014; Wang et al., 2020). In other words, all Chinese stalagmite oxygen isotopes are influenced by both the upstream moisture source and rainout effect along the moisture transport pathway, which are related to the intensity of the ASM (Liu et al., 2020; Zhang et al., 2019). Nevertheless, the contribution of variability in local hydrology cannot be ignored, as stalagmite $\delta^{18}O$ records from different caves do show significant differences at interannual-interdecadal scales. In fact, the stalagmite $\delta^{18}O$ record in the Chinese monsoon region is the result of the superposition of large-scale atmospheric circulation (remote effect signals) and precipitation (local signals) (Wang et al., 2022; Jin et al., 2023).

Integrated analysis through the establishment of inter-regional stalagmite records is an important approach for further interpreting the stalagmite $\delta^{18}O$ record. Principal component analysis (PCA) is a statistical procedure for identifying hypothetical variables (components) that account for the most possible variance in multivariate data (Davis, 1986; Legendre and Legendre, 1998). Recent studies have successfully used PCA to extract common signals from stalagmite records as representative of ASM intensity (Jin et al., 2023; Wang et al., 2022; Yang et al., 2019) or changes in large-scale atmospheric circulation (Zhang et al., 2022). Since the stalagmite $\delta^{18}O$ record provides a mixed signal of atmospheric circulation and local precipitation, removing the circulation signal from the $\delta^{18}O$ record can theoretically allow the extraction of the signal of local hydroclimate change from each individual $\delta^{18}O$ record. Recently, Wang et al. (2022) successfully separated the monsoon and precipitation signals over the last millennium based on three high-resolution stalagmite $\delta^{18}O$ records. However, their study focused on the variabilities in the monsoon and precipitation patterns and was unable to fully achieve the reconstruction of local precipitation.

This study proposes a novel approach for separating the ASM and local rainfall variability from the stalagmite $\delta^{18}O$ record in Eastern China. Stalagmite $\delta^{18}O$ records were collected from the East Asian monsoon region (Fig. 1), from which the monsoon signal was extracted using PCA. The monsoon signal was then deducted to reconstruct changes in hydrological climate in Northern China (NC), Central China (CC), and Southwest China (SWC). This study offers a novel method which is helpful for better interpreting the stalagmite $\delta^{18}O$ record and attempts to understand the physical mechanism of the monsoon-precipitation relationship, and the results could improve predictions of future climate.

2. Data and methods

2.1. Collection of stalagmite records

This study collected 17 published stalagmite $\delta^{18}O$ records from 16 caves (Fig. 1A–Table 1). The caves were selected based on the requirements of a resolution less than 20 years during the last millennium and a distribution covering NC, CC, and SWC. While Karst systems also exist in north-western China and the Tibetan Plateau, matching the records of other caves presents a challenge due to the paucity of records from these areas and the influence of westerly water vapor. Although this study did not include all caves in the monsoon zone, the 16 high-resolution caves that have been published to date have a spatial density that allows the separation of monsoon and regional precipitation variability effectively.

The time span of each stalagmite $\delta^{18}O$ record at least exceeds 500 years (Fig. 1B). Most of the records have been dated based on high precision ^{230}Th-dating and layer counting. However, some caves have dating errors exceeding 20 years (Dong et al., 2018), which should be treated with caution.

2.2. Principal component analysis

This study applied principal component analysis (PCA) to extract common signals from individual caves. The PCA derived new variables that are linear combinations of the original variables. The hypothesis is that the most important components are correlated with other underlying variables. In comparison to other long-term paleoclimate archives, stalagmite $\delta^{18}O$ records in Eastern China have a higher resolution and

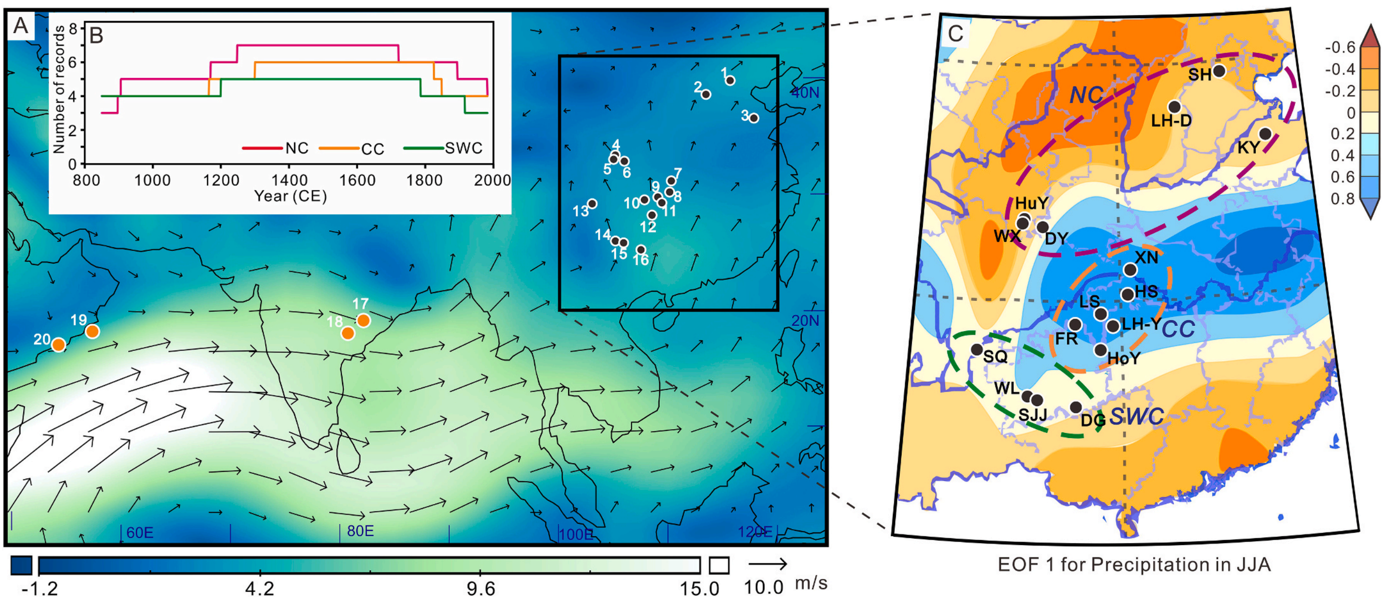

Fig. 1. Location map of Caves in Eastern China and other relevant sites. A. The 16 caves mentioned in this study: 1. SH - Shihua Cave (Wan et al., 2011), 2. LH-D-Lianhua Cave (Dong et al., 2018), 3. KY- Kaiyuan Cave (Wang et al., 2016), 4. HuY- Huangye Cave (Tan et al., 2011), 5. WX- Wanxiang Cave (Zhang et al., 2008), 6. DY - Dayu Cave (Tan et al., 2009), 7. XN- Xiniu Cave (Zhao et al., 2021), 8. HS - Heshang Cave (Wang et al., 2018), 9. LS - Luoshui Cave (Xue et al., 2020), 10. FR - Furong Cave (Li et al., 2011), 11. LH-Y – Lianhua (Yin et al., 2014), 12. HoY – Hongyan Cave (Duan et al., 2022), 13. SQ – Shenqi Cave (Tan et al., 2018), 14. WL - Wulu Cave (Zhao et al., 2020), 15. SJJ – Shijiangjun Cave (Li et al., 2021), 16. DG – Dongge Cave (Wang et al., 2005) are marked by black dots, with the main feature of the Asian summer monsoon in this region. Smaller arrows reflect moisture transport pathway and direction averaged over the whole atmosphere. The JJA moisture transport field during the 1960–2020 CE was generated by NCEP/NCAR reanalysis datasets (https://www.esrl.noaa.gov). **B.** The number of records in northern China (NC), central China (CC) and southwestern China (SWC). At least three or more records exist for all periods in all three areas, and the largest number of records cover the 1300s–1800s phase. **C.** Empirical orthogonal function (EOF) analysis of observed climate data from 1951 to 2012 CE indicates that the spatial and temporal patterns of precipitation variability in Eastern China exhibit a tripolar structure. We added the sites on the map based on *The Third National Report on Climate Change of China*.

Table 1
The information of 16 caves mentioned in this study.

Caves	Location	A.S.L./m	Dating	Resolution/yr	Time span/CE	References
Shihua (SH)	39°47′N, 115°56′E	251	layer counting + U–Th	~5	906-1983	Wan et al. (2011)
Kaiyuan (KY)	36°24′N, 118°02′E	165	layer counting + U–Th	~5	897-1894	Wang et al. (2016)
Lianhua (LH-D)	38°24′N, 113°48′E	1200	U–Th	4–32	850-1983	Dong et al. (2018)
Huangye (HuY)	33°35′N, 105°07′E	1650	U–Th	3–20	850-1983	Tan et al. (2011)
Wanxiang (WX)	33°19′N, 105°00′E	1200	U–Th	1–4	850-1983	Zhang et al. (2008)
Dayu (DY)	33°08′N, 106°18′E	870	U–Th	0.3–3	1248-1982	Tan et al. (2009)
Xiniu (XN)	31°31′N, 110°34′E	1900	U–Th	0.5–3	1165-1848	Zhao et al. (2021)
Heshang (HS)	30°27′N, 110°25′E	294	layer counting + U–Th	1	850-1983	Wang et al. (2022)
Luoshui (LS)	29°43′N, 109°06′E	975	U–Th	3–12	850-1825	Xue et al. (2020)
Furong (FR)	29°13′N, 107°54′E	480	U–Th	4–13	850-1983	Li et al. (2011)
Lianhua (LH-Y)	29°09′N, 109°33′E	459	U–Th	1–3	1300-1983	Yin et al. (2014)
Shenqi (SQ)	28°56′N, 103°05′E	1400	U–Th	3–14	850-1983	Tan et al. (2018)
Hongyan (HoY)	28°06′N, 109°09′E	389	U–Th	2.8	850-1983	Duan et al. (2022)
Wulu (WL)	26°30′N, 105°50′E	1440	U–Th	1–8	850-1916	Zhao et al. (2020)
Shijiangjun (SJJ)	26°17′N, 106°03′E	1300	U–Th	0.5–1	1200-1786	Li et al. (2021)
Dongge (DG-DA)	25°17′N, 108°05′E	680	U–Th	2–11	850-1983	Wang et al. (2005)
Dongge (DG-DX)	25°17′N, 108°05′E	680	layer counting + U–Th	1	850-1983	Zhao et al. (2015)

provide more accurate dating. These advantages of the stalagmite $\delta^{18}O$ records allow PCA to extract common signals within certain errors. More importantly, the selected stalagmite records cover most areas of eastern China and could provide sufficient replications for longer timescale paleoclimate networks. However, the low resolution of some stalagmite $\delta^{18}O$ records as well as dating errors hinder the accurate extraction of the first principal component (PC1). Therefore, three criteria were used to select stalagmite $\delta^{18}O$ records for PCA analysis: (1) as long a record as possible, covering at least the complete MCA period and the LIA period; (2) sufficiently numerous and accurate dating points, with priority given to records derived through annual layer-counting; (3) a sufficiently high resolution averaging <10 years. Based on the above criteria, only seven records from six caves could meet the requirements, which are Huangye Cave (HuY) and Wanxiang Cave (WX) from NC, Heshang Cave (HS), and Furong Cave (FR) from CC and Wulu Cave (WL) and Dongge Cave (DG) from SWC. It should be noticed that there are two stalagmite records (DA (Wang et al., 2005) and DX (Zhao et al., 2015))from Dongge Cave. While the stalagmite $\delta^{18}O$ record from Shihua Cave (SH) was comparatively shorter (Wan et al., 2011), the record satisfied the three criteria. Therefore, this record was considered when examining the reliability of the PCA results. Prior to application of the PCA, the stalagmite records were subjected to yearly interpolation.

Application of PCA to extract the ASM index from stalagmite $\delta^{18}O$ records also allowed the variance percentage (loading) of each stalagmite record and its contribution to different PC series to be obtained. The values of each loading to different principal components (PCs) revealed different correlations between each original record and the PCs. These correlations could be regarded as the weighted contribution of each stalagmite δ^{18}O record to PCs. Therefore, universal positive or negative loadings in any individual PC indicate the influence on that PC by a common factor. Since the loadings of the first principal components (PC1) of stalagmite δ^{18}O records were all positive (Table 2), the PC1 should represent the ASM signal. The ASM index was obtained by weighting each original record based on its loading value, following which the index was multiplied by the explained variance:

$$ASMI = \frac{\sum(S_i \times L_i)}{\sum L_i} \times R^2 \tag{1}$$

where ASMI is the ASM index, S_i is the anomaly of stalagmite δ^{18}O records, L_i is the loading value of each individual stalagmite δ^{18}O records, and R^2 is the explained variance of each PCA result. The unit for ASMI is permil (‰, PDB). In addition, it should be emphasized that ASMI indicates changes in moisture in upstream regions of the water vapor transport pathway (Wang et al., 2020).

It should be noted that even cave records that are not involved in PCA could be used in the local hydroclimate reconstructions below.

2.3. Reconstruction of precipitation

Factors affecting the stalagmite δ^{18}O record can be divided into two categories: 1) Remote effect signals: the processes occurring prior to monsoon-transported water vapor reaching caves in Eastern China are related to ASM intensity, including the water vapor source effect (Tan, 2014), upstream convection (Wang et al., 2020) and the "rainout effect" (Hu et al., 2008). 2) Local hydroclimatic signals: there include changes in local summer precipitation (Zhang et al., 2008; Zhao et al., 2020), and evaporation (Cai and Tian, 2016). Increased local or regional rainfall likely leads to strong Rayleigh fractionation and more negative δ^{18}O values, e.g., the precipitation amount effect. At the same time, increased rainfall results in high relative humidity and weak evaporation, which in turn leads to more negative δ^{18}O values. In other words, any single stalagmite δ^{18}O record must contain information mixed with large-scale atmospheric circulation and local precipitation. Thus, by deducting these remote effects from each stalagmite record, the local precipitation signal can be obtained. Although the ASMI was derived from only seven high-resolution records, it was applicable to the entire monsoon region. Therefore, local precipitation variations could be obtained after subtracting the ASMI from the stalagmite δ^{18}O records.

The local precipitation index (PRI) was reconstructed as the individual cave δ^{18}O records minus the ASMI:

$$PRI = S_i - ASMI \tag{2}$$

where PRI is the precipitation index; S_i is the anomaly of stalagmite δ^{18}O records. PRI and S_i share a same unit (‰, PDB) with ASMI.

3. Results

3.1. Extraction of the monsoon signal from stalagmite records

The current study conducted three PCAs on seven records ($ASMI_{syn-7}$), six records ($ASMI_{syn-6}$), and five records ($ASMI_{syn-5}$), respectively (Table 2). The loadings of the PCA results indicated positive contributions of all stalagmite δ^{18}O records from different caves to PC1 (Table 2). This result suggested that PC1 reflects a common factor in these records and was confirmed by pseudo-proxy experiments utilizing the results of isotopic-enabled climate models (Fig. S1B). Previous studies have shown that variations in stalagmite isotope records in this region mainly reflect upstream convective activity (Wang et al., 2020). In addition, both the observations and reconstructed indices of upstream monsoon changes also demonstrate similar variations to PC1 (Wu, 2005; Zhou et al., 2010). The results confirmed that the common signal (PC1) was consistent with changes in circulation in the upstream water vapor path (Fig. S1C). This results further indicate that common variations in stalagmites δ^{18}O records reflect upstream changes in moisture associated with ASM activity.

The different PC1 series derived from 5 to 7 records show consistent long-term change (Fig. 2A), thereby confirming the method employed in this study. Because all PC1s could show the variation of ASM, we decided to utilize the $\delta^{18}O_{syn-5}$ record with the longest length and

Table 2
The loadings and variances of each PCA results.

	HuY	WX	HS	FR	DX	DA	SH	% variance
PCA_{7syn}	0.41	0.36	0.13	0.42	0.45	0.43	0.35	24.75
PCA_{6syn}	0.42	0.30	0.15	0.48	0.49	0.48	–	32.90
PCA_{5syn}	0.56	0.45	0.24	0.39	0.53	–	–	31.40

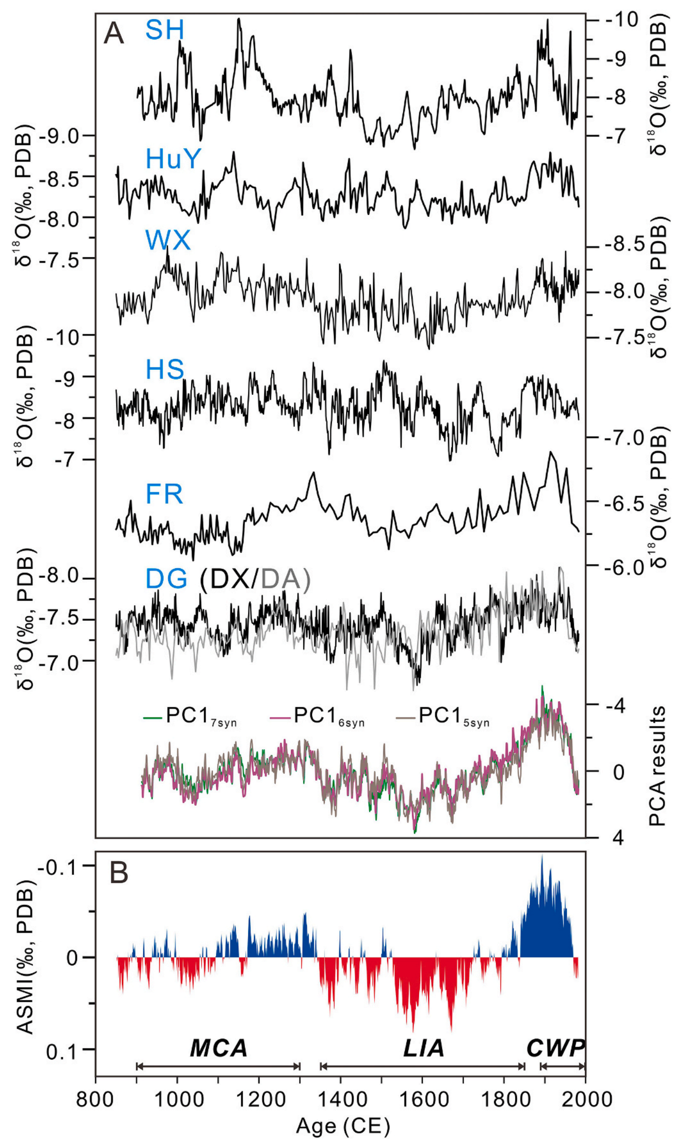

Fig. 2. The seven δ^{18}O records of stalagmite from 6 caves used to principal component analysis (PCA) and their PC1 results. A. Records of stalagmites involved in PCA and their results (see Methods). **B.** The Asian Summer monsoon index (ASMI) series. The blue (red) shading represents strong (weak) monsoons, respectively.

highest resolution to calculate and reconstruct the variability in precipitation in each area (Fig. 2B). We assessed the impact of different interpolation methods on resultant ASMI by interpolating the original stalagmite records to 20-year-resolution sequences, following which they were compared to the yearly interpolation resolution results. Coherent variation could be observed in these two PC1 time series with different temporal resolutions (Fig. S2), which means the uncertainties brought by different interpolation methods could be ignored.

Three stages were identified within ASMI series by different variations. During the MCA period, the negative ASMI indicated a stronger Asian monsoon. Subsequent the 1350s, the ASMI rapidly transitioned to positive until the ~1800s, corresponding exactly to the LIA period. This result is consistent with those provided by the different proxies (Lan et al., 2020). Lastly, ASMI experienced rapid negative changes during the current warm period (CWP). In addition, the records in the current study show several significant weak monsoon phases in the 860s, 910s, 930s, 1030s, 1160s, 1380s, 1440s, 1470s, 1540s–1620s, 1670s, 1710s, 1750s, 1790s, 1840s, and 1980s.

3.2. Reconstruction of precipitation from stalagmite records

PRIs for the 16 caves were obtained by subtracting ASMI from the individual stalagmite $\delta^{18}O$ records. This study accounted for the length and regional representation of individual records by averaging the records according to different regions. The results were regarded as regional precipitation records, with SH, KY, LH-D, HuY, WX, and DY in northern China (NC, Fig. 1C), XN, HS, LS, FR, LH-Y, and HoY in central China (CC, Fig. 1C), and SQ, WL, SJJ, and DG in south-western China (SWC, Fig. 1C).

The reconstructed rainfall in NC shows strong oscillations, particularly prior to the 18^{th} century. Rainfall amount during the MCA and CWP significantly exceeded those in the LIA (Fig. 3A). The driest period

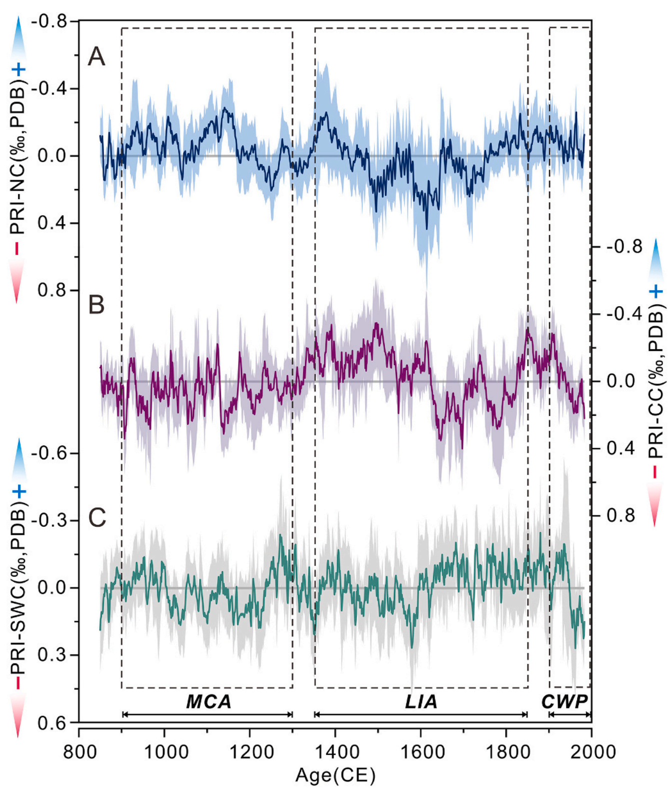

Fig. 3. Precipitation reconstruction from the Eastern monsoon region of China. The reconstructions of NC, CC and SWC precipitation during the 850-1983 CE are shown in A, B and C, respectively. The uncertainties of PRI reconstruction are also shown in shadows.

occurred from the 15^{th} to the 17^{th} century in NC. Reconstructed results for CC indicate that the highest rainfall amount over the last millennium occurred between the 14^{th} and 16^{th} centuries, whereas the drier period occurred during the MCA and the second half of the LIA. Moreover, precipitation of CWP showed a continuous decreasing trend (Fig. 3). Similar to that in CC, rainfall amount during the MCA and CWP were less than that during the LIA in SWC. However, the SWC region was drier in the first half of the LIA phase and wetter in the second half of the LIA phase, opposite to the pattern seen in region CC (Fig. 3C). In summary, during warm (MCA and CWP) periods, rainfall amount was consistently drier in CC and SWC, whereas they were wetter in NC. During cold periods, the CC experienced wet then dry conditions, opposite to the pattern observed in SWC, whereas NC was generally dry.

4. Discussion

4.1. Uncertainties in PRI reconstruction

There were four sources of uncertainty affecting the reconstruction of PRI: (1) analytical errors in the stalagmite isotope record (ε_1); (2) error in the monsoon reconstruction (ε_2); (3) standard deviations (SD_s) resulting from the integration of stalagmites in the various caves; (4) cumulative chronological error in the stalagmite records (SD_{ch}). Analytical error (ε_1) of stalagmites is generally 0.15‰, whereas the cumulative chronological error in the stalagmite records for NC, CC and SWC were 16a, 32a, and 22a, respectively.

PRI was reconstructed by subtracting ASMI from each stalagmite $\delta^{18}O$ record. Therefore, error due to the calculation of ASMI from different numbers of stalagmite $\delta^{18}O$ records needed further evaluation. Sine this study used three calculations of ASMI ($ASMI_{syn-5}$, $ASMI_{syn-6}$, and $ASMI_{syn-7}$), three precipitation reconstructions (PRI_{syn-5}, $PRI_{\ syn-6}$, and $PRI_{\ syn-7}$) were available in NC, CC, and SWC. We evaluated differences between the PRI reconstructions through comparison and correlation analysis. PRI reconstructions based on different ASMI sequences were nearly identical in all three areas (Fig. S3). Variances of the PRI reconstructions for NC, CC, and SWC all exceeded 95%, implying <5% differences in calculations from the different ASMIs. Moreover, a standard deviation of 0.008‰ was obtained for the three sequences (ε_2). This result confirmed the feasibility and reliability of the three ASMI sequences. Furthermore, it can be inferred that regardless of increasing $\delta^{18}O$ records used in the ASMI reconstruction or further high-resolution studies, their impact on the reconstruction of precipitation would be generally negligible. Finally, considering its high resolution, this study used the precipitation reconstruction based on the $ASMI_{syn-5}$ to represent precipitation in the three regions.

Secondly, we evaluated the error in the reconstructed PRI according to the cumulative chronological error in the stalagmite records by shifting the stalagmite records off the ASMI chronology for −16, −8, 0, +8, and +16 years in $\delta^{18}O$ records of NC; −32, −16, 0, +16, and +32 years in $\delta^{18}O$ records of CC; and −22, −11, 0, +11, and +22 years in $\delta^{18}O$ records of SWC. We then averaged all five sets of $\delta^{18}O$ records from the three regions and calculated their standard deviations (SD_{ch}).

Finally, we calculated the uncertainty in the PRI reconstruction by combining the standard deviation from stalagmite isotope integration (SD_s) and the above error values according to Eq. (3) (Wu et al., 2023; Jin et al., 2023), with the results shown as the shaded area in Fig. 3.

$$PRI\ error = \sqrt{\frac{\varepsilon_1^2 + \varepsilon_2^2 + SD_s^2 + SD_{ch}^2}{N-1}} \tag{3}$$

where N is the number of errors (4 in this study). ε_1 , ε_2 , SD_s and SD_{ch} are described above.

4.2. Variations in ASM during the last millennium

Previous studies have shown that upstream precipitation and convective activity can isotopically deplete lower tropospheric water vapor prior to rainout over the cave sites (Cai et al., 2017; Wang et al., 2020). More specifically, summer precipitation $\delta^{18}O$ in Eastern China is mainly delivered by ASM circulation from the Indian Ocean, including the Arabian Sea, the Bay of Bengal, and other surrounding areas. Our study confirmed the reliability of the reconstructed ASMI record by comparing with other ASM-related hydroclimatic records of upstream of water vapor, from central Indian cave stalagmites (Sinha et al., 2011), Arabian Sea sediments (Anderson et al., 2002) and the Qunf Cave stalagmite record (Fleitmann et al., 2007) (Fig. 4), which showed close relationships between the ASMI results of this study and those from the upstream regions (Fig. 1A). The anomaly in ASMI was inversely related to the intensity of the ASM.

The results of wavelet transformation and spectral analyses of ASMI show significant ~11-yr, 17–21-yr, and ~200-yr cycles, with the 200-yr cycle prevailing throughout the past millennium (Fig. S4), suggesting the influence of a long-term driver on ASMI. Variation in ASM was strongly consistent with change in effective solar radiation (ESR) and interhemispheric temperature at a centennial scale. Increased ESR enhanced the contrast between continental and oceanic thermal conditions. A greater proportion of continents in the Northern Hemisphere contributed to an increase in inter-hemispheric temperature, leading to

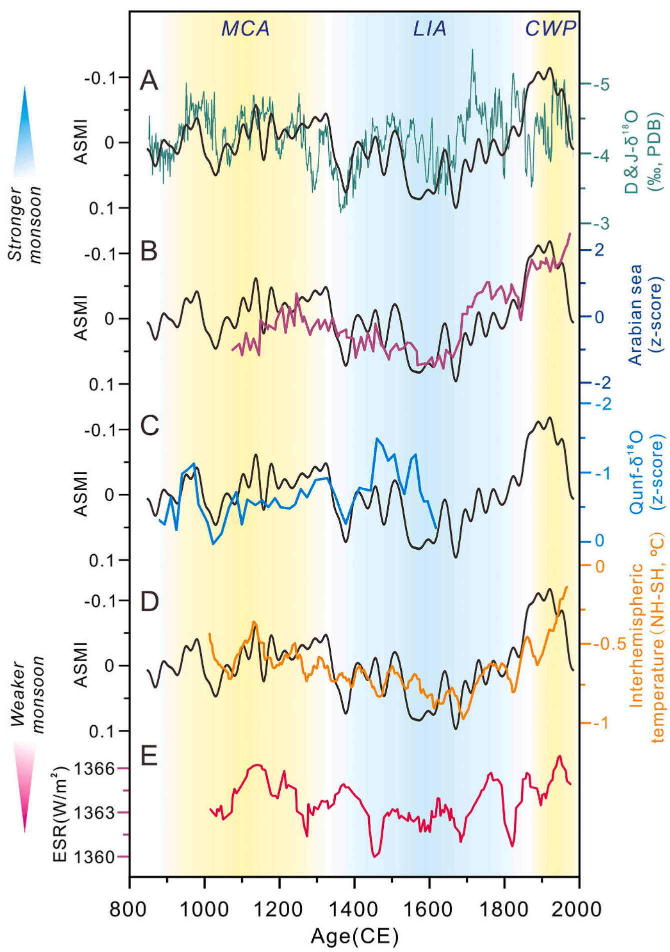

Fig. 4. Comparisons of ASMI (30-year smoothing of the data) with other records from different regions and climate forcings. A. The composite $\delta^{18}O$ time series from Jhumar Cave and Dandak Cave (Sinha et al., 2011). **B.** The *G. bulloides* abundance from Arabian Sea sediment box core RC2735 (Anderson et al., 2002). **C.** The stalagmite $\delta^{18}O$ time series from Qunf Cave (Fleitmann et al., 2007). **D.** The inter-hemispheric temperature sequence (Liu et al., 2009). **E.** The time series of effective solar radiation (ESR) (Liu et al., 2009). The periods of MCA, LIA and CWP are highlighted.

a consequent enhancement in the ASM (Liu et al., 2009; Neukom et al., 2014) (Fig. 4; Fig. S5).

However, the ASM declined rapidly after the 1920s at a rate unprecedented in the last millennium. This decline can be related to anthropogenic actions. The increase in CO_2 over the past century has contributed to rapidly increasing temperatures in the Southern Hemisphere along with a significantly strengthened trade wind (Perren et al., 2020), which collectively triggered a weakening in the ASM. This weakening ASM coupled with the stagnation of temperature in the Northern Hemisphere became more prominent in the 1940s–1970s, led to decreasing interhemispheric temperature, and potentially exacerbated the effects of human activity. Ding et al. (2009) suggested that the weakening of the ASM was dominated by a significant weakening of the easterly rapid component of the tropical highs induced by cooling in the upper mid- and high-troposphere and possible warming in the lower latitudes of Asia. In addition, some studies have pointed to a possible correlation between the monsoonal recession seen over recent decades and the Southern Oscillation Index (SOI) (Zhang et al., 2022). Recently, Zhao et al. (2023) suggested that the decline in the Atlantic Meridional Overturning Circulation (AMOC) coinciding with the period of global warming may play a crucial role in the weakening of the ASM. In summary, centennial-scale variations in ASM might be related to changes in the differences in temperature between the Northern and Southern hemispheres triggered by changes in ESR. In contrast, the rapid decline in the monsoon over recent decades may have been influenced by both natural (e.g., SOI and AMOC) and anthropogenic forcings.

We further applied multiple liner regression (MLR) analyses to assess the relative contributions of individual climate drivers (Wang et al., 2017). Factors considered included solar activity (Delaygue and Bard, 2011), Atlantic Multidecadal Oscillation (AMO) (Wang et al., 2017), Pacific Decadal Oscillation (PDO) (Mann et al., 2009), and CO_2, representing the roles of external forcing, North Atlantic SST, Pacific SST, and human activities, respectively. The results of MLR analyses showed that the main driver of ASMI prior to industrialization was solar activity (1850 CE), whereas the contributions of AMO, PDO, and human activities increased after industrialization (Fig. S6). These results are largely consistent with the above findings , suggesting that the monsoon-related drivers have temporal dependencies. As mentioned above, centennial-scale solar activity is the dominant forcing, whereas at interannual-interdecadal scales, internal variability influences the monsoon through air-sea interactions. For example, during the El Niño phase, anomalous warming sea surface temperature (SST) in the central-eastern tropical Pacific and the more intense upward air masses are transferred to the warm waters. Consequently, convection is suppressed in the western Pacific, tropical Indian Ocean and surrounding regions, and intensified in the central and eastern Pacific relative to the normal phase (Cai et al., 2017; Wang et al., 2020). This in turn leads to the weakening of the monsoon. Overall, synergies between internal and external drivers on different time scales regulate the variability of the ASM.

4.3. *Comparison of reconstructed precipitation with other hydroclimatic records*

We compared reconstructed precipitation with local observational records of precipitation (Fig. 5). The reconstructed rainfall series for the three regions followed a trend that is consistent with the reconstruction of drought and flood (D/F) (Qian et al., 2011) and model simulations (Shi et al., 2021) over the past millennium (Fig. 5A and B), although there are also some discrepancies between the results of this study and other records. For instance, our results show a wetter background around 1750 CE in CC, which contradicts that of model simulations (Fig. 5E). Nevertheless, the reconstruction of drought and flood showed a wetter condition between the 1580s–1620s, which is consistent with our results (Fig. 5D). Other records also allude to a wetter condition in

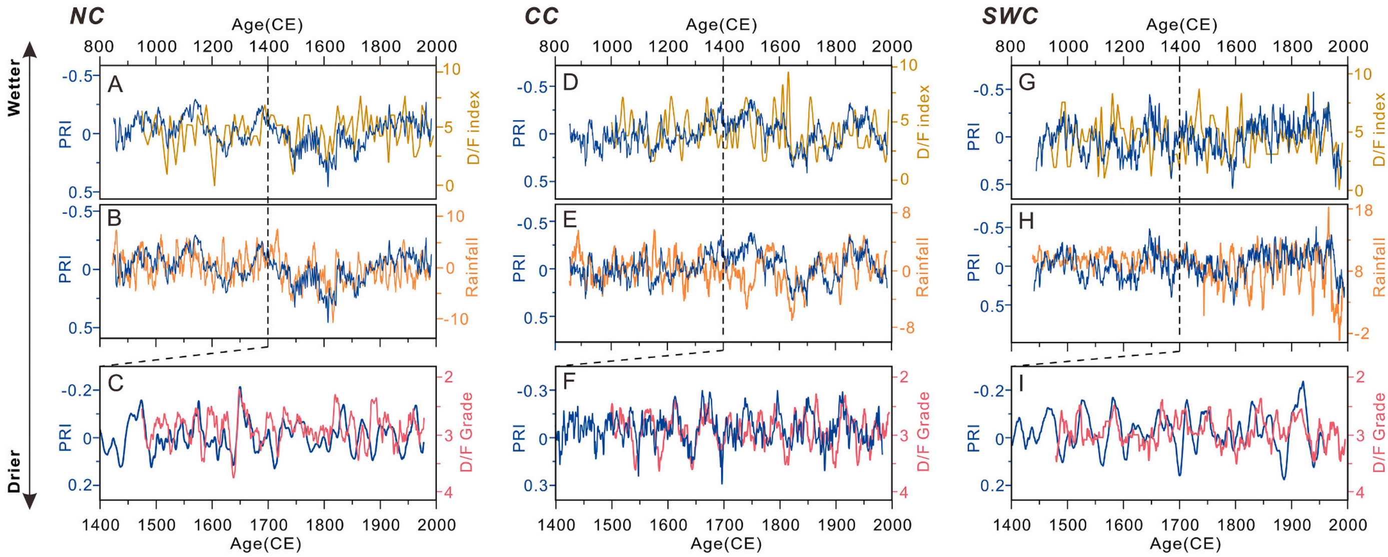

Fig. 5. Comparisons among precipitation reconstruction index (PRI) from Eastern China of this study with other records in three regions. A, D and G. Comparisons of PRI and Dry/Flood (D/F) index records in three regions (Qian et al.,.2011), where higher values of the D/F index are wetter. **B, E and H.** Rainfall derived through modeling for northern China (NC), central China (CC), and southwestern China (SWC), respectively (Shi et al., 2021). **C, F, and I.** the D/F grade from historical documented records (Zheng et al., 2006). Note that the smaller D/F grade ratings point to wetter conditions. Considering that the D/F have only 5 levels, and the PRI were processed by 0.01-high pass filtering.

central China from the 14th to 16th centuries (Duan et al., 2020). The reconstructed rainfall for SWC is also in general agreement with the simulated rainfall and D/F reconstruction (Fig. 5G and H). The trends of drier and wetter conditions during the MCA and LIA periods in SWC, respectively, are consistent with variations in precipitation inferred from changes in water level of Lake Chenghai, Yunnan, southwestern China (Xu et al., 2019). The differences between the results of this study and the model simulations can be attributed to different study areas, uncertainty associated with age, and the errors in the simulated rainfall for this region before 1500 CE (Shi et al., 2021). Since there are some inter-decadal differences in reconstructed precipitation and other records for the three regions, we then compared the reconstructed precipitation with in this study with drought/flood levels in historical documented records (Zheng et al., 2006) (Fig. 5C–F, I). The results show that the reconstructed precipitation in our study is remarkably consistent with the reconstructions of drought and flood grade over the last 500 years. This consistency further confirms the reliability of the reconstructed precipitation as well as the accuracy of the reconstructed chronology, at least during the last 500 years.

In summary, this study presents a novel approach that successfully separated the monsoon and local precipitation from the stalagmite $\delta^{18}O$ records and provided a long-term, high-resolution reconstruction of the monsoon and precipitation records for Eastern China. By verifying the reconstructed precipitation against pre-existing precipitation records from different paleoclimatic proxies, we believe that the method is applicable to longer time scales or larger scales. Importantly, since the ASMI and the PRI in Eastern China were synchronously reconstructed from the same set of samples, there was no chronological difference between the ASMI and PRI, and this represents a key prerequisite for investigating the relationship between the monsoon and precipitation.

4.4. Links between the ASM and precipitation in Eastern China

Published paleoclimatic studies suggested a stronger monsoon during the MCA than during the LIA (Liu et al., 2011; Zhang et al., 2008). However, the reconstructed precipitation in this study along with previous studies suggest a “dry southern and wet northern” patter during the MCA and an opposite pattern during the LIA at large regional scales. The influences of climatic drivers and internal variability likely contribute to the complex relationship between the monsoon and precipitation (ASM-precipitation relationship) in different regions (Shi et al., 2018). These relationships remain unclear due to differences in dating between the archives and the limitations of resolution. We examined the ASM-precipitation relationship at a sub-centennial scale using monsoon and precipitation reconstructions along a common chronology. A 101-year running correlation was used to explore the ASM-precipitation relationship among the different periods during the last millennium.

In NC, the correlation (r) varied from −0.85 to 0.80 in recent 1000 years, indicating a strong relationship between monsoon and precipitation showing a temporal variability. At the 95% confidence level (shaded area in Fig. 6), the ASM-precipitation relationship was significantly positive between the 1000s–1100s, 1450s, and 1700s–present, whereas it was significantly negative during the 1150–1400s and 1500–1700s.The trend evident in this result is opposite to that in the phase change of NAO ($r = -0.4$, $p < 0.01$) (Trouet et al., 2009). The phase of NAO is inversely related to the ASM-precipitation relationship. We propose that the NAO influences the ASM-precipitation relationship by modulating the position of the East Asian Westerly Jet (EAWJ). The warm phases of NAO correspond with the southward jet flow pattern around the mid-latitudes, which accelerates subsidence over the northern area of the jet stream and suppresses convective precipitation in the following summer (Sung et al., 2006). While this observation explained the strong monsoon during the late-MCA period (1200–1400s), the ASM-precipitation moving correlation coefficient was significantly negative. In contrast, the ASM was weak during the LIA, and the transition of NAO to a negative phase may enhance precipitation in NC (Chen et al., 2006), thereby possibly explaining the negative ASM-precipitation moving correlation during the LIA. In addition, increased precipitation occurred in the NC during the negative phase of NAO and strong ASM during the early-MCA period (before the 1100s) and the CWP period, during which there was a significantly positive relationship between ASM and precipitation.

The temporal changes in ASM were particularly consistent with those in precipitation in CC over some periods, whereas this relationship was weaker over other periods. This result suggests a non-stationary relationship between ASM and precipitation in CC. As shown in Fig. 6, those significant correlations were almost positive, including during the

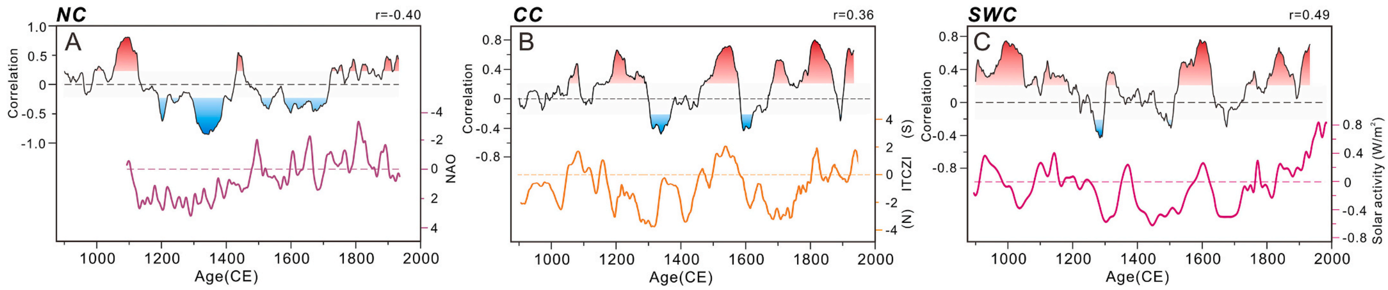

Fig. 6. 101-year running correlation between ASMI and PRI in three regions of China and links to the climate factors. The NAO (Trouet et al., 2009) (**A**), ITCZ (Tan et al., 2019) (**B**) and solar radiation (Delaygue and Bard, 2011) (**C**) show significant agreements with ASM-precipitation relationships in NC, CC and SWC, respectively. Shadows represent more than 95% confidence levels.

~1050s, 1100–1300s, 1450–1560s, and 1650s–present. Nevertheless, phases of negative correlations also occurred in the 1290s–1350s and ~1600s. The moving correlation curve show a strong correlation with the intertropical convergence zone (ITCZ) index ($r = 0.36$, $p < 0.01$) (Tan et al., 2019), indicating that the variations in the ASM-precipitation relationship in CC were consistent with the meridional ITCZ shifts. The negative correlations between ASM and precipitation can possibly be attributed to the northward shift of ITCZ. Northward movement of the ITCZ enhances the cross-equatorial airflow, thereby providing a large source of water vapor for the development and persistence of heavy rainfall, whereas some low-pressure systems or typhoons in the ITCZ can move directly northward, bringing abundant water vapor and heavy rainfall (Ding, 2019). These observations can be related to the presence of atmospheric rivers originating from the tropics and their role in global rainstorms, which have been identified and emphasized in recent studies (Guan and Waliser, 2015). Sustained precipitation triggered by an active (northward moving) ITCZ may be important for decoupling the monsoon and precipitation, for example around the 1300s, 1600s, and 1900s. However, these disturbances may be relatively small and present only in individual periods as studies have generally assumed that the ASM-precipitation relationship in the CC is impacted by the movement of the Meiyu front (Zhang et al., 2018).

The ASM-precipitation relationship is stable in SWC, with a generally positive correlation between ASM and precipitation, except during three periods: ~1300s, ~1500s, and ~1670s. The moving correlation curve over the past millennium agrees well with changes in solar irradiation ($r = 0.49$, $p < 0.01$) (Delaygue and Bard, 2011), In addition, the major long-term negative phases of the moving correlation coincided exactly with the three periods of minimum solar activity (Fig. 6). Besides for over these three periods, the ASM-precipitation relationship essentially presented a stable positive correlation, suggesting that monsoon strength may present a consistent control on precipitation. Strengthening of the ASM coincides with increased transport of water vapor by the monsoon and increased precipitation in the SWC region and vice versa. This relatively stable correlation was also identified in the climate model simulations (Shi et al., 2018). However, the model simulations did not reflect the negative correlation during periods of solar minimum. We propose that intervening factors, such as sea surface temperature (SST) of the northern-Pacific and internal variability (e.g., PDO) may lead to a weak or even negative ASM-precipitation correlation during the solar minimum periods. For example, differences between oceanic and terrestrial heat capacity resulted in a decrease in solar activity, leading to a corresponding drop in land temperature, which in turn resulted in weakening of the ASM. At the same time, the differences in the monsoon and precipitation between positive PDO and negative PDO phases also decreased (Xue et al., 2023). These less significant differences may have influenced precipitation by regulating anticyclonic circulation patterns in the 850 hPa over SWC, which eventually resulted in precipitation decoupling from the ASM.

In summary, the results of moving correlation shows a non-stationary ASM-precipitation relationship at sub-centennial scales, which may be related to the movement of rainbands in the East Asian monsoon region, and be subject to the complex effects of multiple climatic factors. This study identifies these climatic fingerprints, thereby guiding future research. Nevertheless, the correlation coefficients (r) between ASM and precipitation during the last millennium in the NC, CC, and SWC regions were only 0.32, 0.17, and 0.29, respectively. These correlations suggest that the monsoon and precipitation showed similar trends in NC and SWC over the past millennium, consistent with previous understanding (Liu et al., 2020). On the other hand, the overall ASM-precipitation correlation in the CC was less significant, possibly due to the more complex and sensitive circulation background of the region. The frequency of extreme compound precipitation events is likely to increase in the future. In addition, variability in ASM was significantly regulated by human activities over the past few centuries since the Industrial Revolution. The likely more frequent decoupling of the monsoon-precipitation linkage will increase the difficulty associated in predicting the characteristics of future distributions of precipitation. Therefore, there is an urgent need for further follow-up studies to obtain a more comprehensive context for climate prediction.

5. Conclusions and outlook

This study applied PCA to successfully separate monsoon and local precipitation based on stalagmite $\delta^{18}O$ records. This study reinterpreted the stalagmite $\delta^{18}O$ signal and provided sufficient data support for examining the ASM-precipitation relationship. The results of our study show that the ASM is significantly related to interhemispheric temperature due to the effects of ESR, SOI, AMOC, and human activities in the ASM during the last century. Our study also reconstructed precipitation in three regions (NC, CC, and SWC) in Eastern China over the past millennium. Significant differences in precipitation were observed between NC, CC, and SWC on a decadal-centennial scale. Furthermore, the comparison of the reconstructed precipitation with existing records confirmed the confidence of the precipitation reconstruction. Subsequently, we examined the ASM-precipitation relationship over the past millennium using monsoon and precipitation series under a common chronology. The ASM-precipitation relationship was unstable under sub-centennial scales and was regulated by NAO, ITCZ, and solar activity in NC, CC, and SWC, respectively. In contrast, the overall positive ASM-precipitation correlation at the millennial scale was observed in NC and SWC, though this relationship was weak in CC regions, possibly due to the different sensitivities of individual regions to climate.

Lastly, we attempted to use the multiplicity of stalagmite records in the Chinese monsoon region as an advantage rather than a disadvantage, with the resulting cross-regional stalagmite $\delta^{18}O$ network suggested to offer a new approach for representing the connection between the ASM and precipitation. The results of this study can help further characterize the monsoon-precipitation relationship at larger temporal and spatial scales.

Credit author statement

C.Y.H.: Conceptualization; Formal analysis; Funding acquisition; Investigation; Methodology; Supervision; Writing - Review & editing. **Z. Y.H.:** Data curation; Formal analysis; Investigation; Methodology; Validation; Visualization; Writing - original draft. **H.W.F.:** Supervision; Formal analysis; Methodology; Supervision; Validation; Writing - review & editing. **Y.H.L.:** Methodology; Writing - review & editing. **Z.P.W: Methodology**

Declaration of competing interest

The authors declare that they have no known competing financial interests or personal relationships that could have appeared to influence the work reported in this paper.

Acknowledgements

We gratefully acknowledge Prof. Bar-Matthews and three anonymous reviewers for their constructive comments. This work was supported by the MOST funding National Key R&D Program of China (2019YFE0125000) and by National Natural Science Foundation of China (42372217).

Data availability

We have shared the link to my data at the Attach File step

Appendix A. Supplementary data

Supplementary data to this article can be found online at https://doi.org/10.1016/j.quascirev.2023.108498.

References

Anderson, D.M., Overpeck, J.T., Gupta, A.K., 2002. Increase in the asian southwest monsoon during the past four centuries. Science 297, 596–599. https://doi.org/10.1126/science.1072881.

Baker, A.J., Sodemann, H., Baldini, J.U.L., Breitenbach, S.F.M., Johnson, K.R., Van Hunen, J., Zhang, P., 2015. Seasonality of westerly moisture transport in the East Asian summer monsoon and its implications for interpreting precipitation δ^{18}O. J. Geophys. Res. Atmospheres 120, 5850–5862. https://doi.org/10.1002/2014JD022919.

Cai, W., Ng, B., Wang, G., Santoso, A., Wu, L., Yang, K., 2022. Increased ENSO Sea surface temperature variability under four IPCC emission scenarios. Nat. Clim. Change 12, 228–231. https://doi.org/10.1038/s41558-022-01282-z.

Cai, Z., Tian, L., 2016. Atmospheric controls on seasonal and interannual variations in the precipitation isotope in the East Asian monsoon region. J. Clim. 29, 1339–1352. https://doi.org/10.1175/JCLI-D-15-0363.1.

Cai, Z., Tian, L., Bowen, G.J., 2017. ENSO variability reflected in precipitation oxygen isotopes across the Asian Summer Monsoon region. Earth Planet Sci. Lett. 475, 25–33. https://doi.org/10.1016/j.epsl.2017.06.035.

Chen, F., Huang, X., Zhang, J., Holmes, J.A., Chen, J., 2006. Humid Little ice age in arid central asia documented by bosten lake, xinjiang, China. Sci. China Ser. Earth Sci. 49, 1280–1290. https://doi.org/10.1007/s11430-006-2027-4.

Chen, J., Chen, F., Feng, S., Huang, W., Liu, J., Zhou, A., 2015. Hydroclimatic changes in China and surroundings during the medieval climate anomaly and Little ice age: spatial patterns and possible mechanisms. Quat. Sci. Rev. 107, 98–111. https://doi.org/10.1016/j.quascirev.2014.10.012.

Cheng, H., Edwards, R.L., Sinha, A., Spötl, C., Yi, L., Chen, S., Kelly, M., Kathayat, G., Wang, X., Li, X., Kong, X., Wang, Y., Ning, Y., Zhang, H., 2016. The Asian monsoon over the past 640,000 years and ice age terminations. Nature 534, 640–646. https://doi.org/10.1038/nature18591.

Davis, J.C., 1986. Statistics and Data Analysis in Geology. John Wiley & Sons.

Delaygue, G., Bard, E., 2011. An Antarctic view of Beryllium-10 and solar activity for the past millennium. Clim. Dynam. 36, 2201–2218. https://doi.org/10.1007/s00382-010-0795-1.

Ding, Y., 2019. The major advances and development process of the theory of heavy rainfalls in China. Torrential Rain and Disasters 38 (5), 395–406. https://10.3969/j.issn.1004-9045.2019.05.001.

Ding, Y., Chan, J.C.L., 2005. The East Asian summer monsoon: an overview. Meteorol. Atmos. Phys. 89, 117–142. https://doi.org/10.1007/s00703-005-0125-z.

Ding, Y., Sun, Y., Wang, Z., Zhu, Y., Song, Y., 2009. Inter-decadal variation of the summer precipitation in China and its association with decreasing Asian summer monsoon Part II: possible causes. Int. J. Climatol. 29, 1926–1944. https://doi.org/10.1002/joc.1759.

Ding, Y., Wang, Z., Sun, Y., 2008. Inter-decadal variation of the summer precipitation in East China and its association with decreasing Asian summer monsoon. Part I: observed evidences. Int. J. Climatol. 28, 1139–1161. https://doi.org/10.1002/joc.1615.

Dong, J., Shen, C.-C., Kong, X., Wu, C.-C., Hu, H.-M., Ren, H., Wang, Y., 2018. Rapid retreat of the East Asian summer monsoon in the middle Holocene and a millennial weak monsoon interval at 9 ka in northern China. J. Asian Earth Sci. 151, 31–39. https://doi.org/10.1016/j.jseaes.2017.10.016.

Duan, F., Zhang, Z., Wang, Y., Chen, J., Liao, Z., Chen, S., Shao, Q., Zhao, K., 2020. Hydrological variations in central China over the past millennium and their links to the tropical Pacific and North Atlantic oceans. Clim. Past 16, 475–485. https://doi.org/10.5194/cp-16-475-2020.

Duan, F., Zhang, Z., Liu, D., Shao, Q., Zhao, K., Wang, Y., 2022. A new stalagmite oxygen isotope record over the last 1350 years: insights into spatial variation in Asian summer monsoon and temperature forcing. Quat. Sci. Rev. 284, 107499 https://doi.org/10.1016/j.quascirev.2022.107499.

Fleitmann, D., Burns, S.J., Mangini, A., Mudelsee, M., Kramers, J., Villa, I., Neff, U., Al-Subbary, A.A., Buettner, A., Hippler, D., Matter, A., 2007. Holocene ITCZ and Indian monsoon dynamics recorded in stalagmites from Oman and Yemen (Socotra). Quat. Sci. Rev. 26, 170–188. https://doi.org/10.1016/j.quascirev.2006.04.012.

Guan, B., Waliser, D.E., 2015. Detection of atmospheric rivers: evaluation and application of an algorithm for global studies: detection of Atmospheric Rivers. J. Geophys. Res. Atmospheres 120, 12514–12535. https://doi.org/10.1002/2015JD024257.

Hao, Z., Zheng, J., Ge, Q., Bai, M., 2023. A 2.5° × 2.5° gridded drought/flood grades dataset for eastern China during the last millennium. Sci. Data 10, 202. https://doi.org/10.1038/s41597-023-02110-5.

Hu, C., Henderson, G.M., Huang, J., Xie, S., Sun, Y., Johnson, K.R., 2008. Quantification of Holocene Asian monsoon rainfall from spatially separated cave records. Earth Planet Sci. Lett. 266, 221–232. https://doi.org/10.1016/j.epsl.2007.10.015.

Jiang, S., Zhou, X., Sachs, J.P., Li, Z., Tu, L., Lin, Y., Liu, X., Chen, A., Shen, Y., 2023. The mean state of the tropical pacific ocean differed between the medieval warm period and the industrial era. Commun. Earth Environ. 4, 74. https://doi.org/10.1038/s43247-023-00734-4.

Jin, X., Hu, C., Hu, Z., Fan, H., Liu, Y., 2023. Weakening monsoon event during 2.8 ka BP in East China linked to the North Atlantic cooling. Quat. Sci. Rev. 306, 108037 https://doi.org/10.1016/j.quascirev.2023.108037.

Lan, J., Xu, H., Lang, Y., Yu, K., Zhou, P., Kang, S., Zhou, K., Wang, X., Wang, T., Cheng, P., Yan, D., Yu, S., Che, P., Ye, Y., Tan, L., 2020. Dramatic weakening of the East Asian summer monsoon in northern China during the transition from the medieval warm period to the Little ice age. Geology 48, 307–312. https://doi.org/10.1130/G46811.1.

Legendre, P., Legendre, L., 1998. Numerical Ecology. Elsevier, p. 853, 2nd English ed.

Li, H., Dai, A., Zhou, T., Lu, J., 2010. Responses of East Asian summer monsoon to historical SST and atmospheric forcing during 1950–2000. Clim. Dynam. 34, 501–514. https://doi.org/10.1007/s00382-008-0482-7.

Li, H., Lee, Z., Wan, N., Shen, C., Li, T., Yuan, D., Chen, Y., 2011. The δ^{18}O and δ^{13}C records in an aragonite stalagmite from Furong Cave, Chongqing, China: a-2000-year record of monsoonal climate. J. Asian Earth Sci. 40, 1121–1130. https://doi.org/10.1016/j.jseaes.2010.06.011.

Li, T., Xiao, S., Shen, C., Zhang, J., Chen, C., Cheng, H., Spötl, C., Huang, R., Wang, T., Li, J., Wu, Y., Liu, Z., Edwards, R.L., Yu, T., 2021. Little Ice Age climate changes in Southwest China from a stalagmite δ^{18}O record. Palaeogeogr. Palaeoclimatol. Palaeoecol. 562, 110167 https://doi.org/10.1016/j.palaeo.2020.110167.

Liu, J., Chen, F., Chen, J., Xia, D., Xu, Q., Wang, Z., Li, Y., 2011. Humid medieval warm period recorded by magnetic characteristics of sediments from Gonghai Lake, Shanxi, North China. Chin. Sci. Bull. 56, 2464–2474. https://doi.org/10.1007/s11434-011-4592-y.

Liu, J., Wang, B., Ding, Q., Kuang, X., Soon, W., Zorita, E., 2009. Centennial variations of the global monsoon precipitation in the last millennium: results from ECHO-G model. J. Clim. 22, 2356–2371. https://doi.org/10.1175/2008JCLI2353.1.

Liu, X., Liu, J., Chen, S., Chen, J., Zhang, X., Yan, J., Chen, F., 2020. New insights on Chinese cave δ^{18}O records and their paleoclimatic significance. Earth Sci. Rev. 207, 103216 https://doi.org/10.1016/j.earscirev.2020.103216.

Mann, M.E., Zhang, Z., Rutherford, S., Bradley, R.S., Hughes, M.K., Shindell, D., Ammann, C., Faluvegi, G., Ni, F., 2009. Global signatures and dynamical origins of the Little ice age and medieval climate anomaly. Science 326, 1256–1260. https://doi.org/10.1126/science.1177303.

Neukom, R., Gergis, J., Karoly, D.J., Wanner, H., Curran, M., Elbert, J., González-Rouco, F., Linsley, B.K., Moy, A.D., Mundo, I., Raible, C.C., Steig, E.J., Van Ommen, T., Vance, T., Villalba, R., Zinke, J., Frank, D., 2014. Inter-hemispheric temperature variability over the past millennium. Nat. Clim. Change 4, 362–367. https://doi.org/10.1038/nclimate2174.

Pausata, F.S.R., Battisti, D.S., Nisancioglu, K.H., Bitz, C.M., 2011. Chinese stalagmite δ^{18}O controlled by changes in the Indian monsoon during a simulated Heinrich event. Nat. Geosci. 4, 474–480. https://doi.org/10.1038/ngeo1169.

Perren, B.B., Hodgson, D.A., Roberts, S.J., Sime, L., Van Nieuwenhuyze, W., Verleyen, E., Vyverman, W., 2020. Southward migration of the Southern Hemisphere westerly winds corresponds with warming climate over centennial timescales. Commun. Earth Environ. 1, 58. https://doi.org/10.1038/s43247-020-00059-6.

Qian, W., Zhu, Y., Tang, S., 2011. Reconstructed index of summer monsoon dry-wet modes in East Asia for the last millennium. Chin. Sci. Bull. 56, 3019. https://doi.org/10.1007/s11434-011-4714-6.

Shekhar, M., Sharma, A., Dimri, A.P., Tandon, S.K., 2022. Asian summer monsoon variability, global teleconnections, and dynamics during the last 1,000 years. Earth Sci. Rev. 230, 104041 https://doi.org/10.1016/j.earscirev.2022.104041.

Shi, F., Lu, H., Guo, Z., Yin, Q., Wu, H., Xu, C., Zhang, E., Shi, J., Cheng, J., Xiao, X., Zhao, C., 2021. The position of the current warm period in the context of the past

22,000 Years of summer climate in China. Geophys. Res. Lett. 48 https://doi.org/10.1029/2020GL091940.
Shi, H., Wang, B., Liu, J., Liu, F., 2019. Decadal–Multidecadal variations of asian summer rainfall from the Little ice age to the present. J. Clim. 32, 7663–7674. https://doi.org/10.1175/JCLI-D-18-0743.1.
Shi, J., Yan, Q., Wang, H., 2018. Timescale dependence of the relationship between the East Asian summer monsoon strength and precipitation over eastern China in the last millennium. Clim. Past 14, 577–591. https://doi.org/10.5194/cp-14-577-2018.
Sinha, A., Berkelhammer, M., Stott, L., Mudelsee, M., Cheng, H., Biswas, J., 2011. The leading mode of Indian Summer Monsoon precipitation variability during the last millennium. Geophys. Res. Lett. 38 https://doi.org/10.1029/2011GL047713.
Sun, L., Shen, B., Sui, B., Huang, B., 2017. The influences of East Asian monsoon on summer precipitation in northeast China. Clim. Dynam. 48, 1647–1659. https://doi.org/10.1007/s00382-016-3165-9.
Sung, M.-K., Kwon, W.-T., Baek, H.-J., Boo, K.-O., Lim, G.-H., Kug, J.-S., 2006. A possible impact of the North Atlantic Oscillation on the east Asian summer monsoon precipitation. Geophys. Res. Lett. 33, L21713 https://doi.org/10.1029/2006GL027253.
Tan, L., Cai, Y., An, Z., Yi, L., Zhang, H., Qin, S., 2011. Climate patterns in north central China during the last 1800yr and their possible driving force. Clim. Past 7, 685–692. https://doi.org/10.5194/cp-7-685-2011.
Tan, L., Cai, Y., Cheng, H., An, Z., Edwards, R.L., 2009. Summer monsoon precipitation variations in central China over the past 750years derived from a high-resolution absolute-dated stalagmite. Palaeogeogr. Palaeoclimatol. Palaeoecol. 280, 432–439. https://doi.org/10.1016/j.palaeo.2009.06.030.
Tan, L., Cai, Y., Cheng, H., Edwards, L.R., Lan, J., Zhang, H., Li, D., Ma, L., Zhao, P., Gao, Y., 2018. High resolution monsoon precipitation changes on southeastern Tibetan Plateau over the past 2300 years. Quat. Sci. Rev. 195, 122–132. https://doi.org/10.1016/j.quascirev.2018.07.021.
Tan, L., Shen, C.-C., Löwemark, L., Chawchai, S., Edwards, R.L., Cai, Y., Breitenbach, S.F. M., Cheng, H., Chou, Y.-C., Duerrast, H., Partin, J.W., Cai, W., Chabangborn, A., Gao, Y., Kwiecien, O., Wu, C.-C., Shi, Z., Hsu, H.-H., Wohlfarth, B., 2019. Rainfall variations in central Indo-Pacific over the past 2,700 y. Proc. Natl. Acad. Sci. USA 116, 17201–17206. https://doi.org/10.1073/pnas.1903167116.
Tan, M., 2014. Circulation effect: response of precipitation $\delta^{18}O$ to the ENSO cycle in monsoon regions of China. Clim. Dynam. 42, 1067–1077. https://doi.org/10.1007/s00382-013-1732-x.
Trouet, V., Esper, J., Graham, N.E., Baker, A., Scourse, J.D., Frank, D.C., 2009. Persistent positive North Atlantic oscillation mode dominated the medieval climate anomaly. Science 324, 78–80. https://doi.org/10.1126/science.1166349.
Wan, N., Li, H., Liu, Z., Yang, H., Yuan, D., Chen, Y., 2011. Spatial variations of monsoonal rain in eastern China: instrumental, historic and speleothem records. J. Asian Earth Sci. 40, 1139–1150. https://doi.org/10.1016/j.jseaes.2010.10.003.
Wang, J., Yang, B., Ljungqvist, F.C., Luterbacher, J., Osborn, T.J., Briffa, K.R., Zorita, E., 2017. Internal and external forcing of multidecadal Atlantic climate variability over the past 1,200 years. Nat. Geosci. 10, 512–517. https://doi.org/10.1038/ngeo2962.
Wang, M., Hu, C., Liu, Y., Li, L., Xie, S., Johnson, K., 2022. Precipitation in eastern China over the past millennium varied with large-scale climate patterns. Commun. Earth Environ. 3, 321. https://doi.org/10.1038/s43247-022-00664-7.
Wang, Q., Zhou, H., Cheng, K., Chi, H., Shen, C.-C., Wang, C., Ma, Q., 2016. The climate reconstruction in Shandong Peninsula, northern China, during the last millennium based on stalagmite laminae together with a comparison to $\delta^{18}O$. Clim. Past 12, 871–881. https://doi.org/10.5194/cp-12-871-2016.
Wang, Y., Hu, C., Ruan, J., Johnson, K.R., 2020. East Asian precipitation $\delta^{18}O$ relationship with various monsoon indices. J. Geophys. Res. Atmospheres 125. https://doi.org/10.1029/2019JD032282.
Wang, Y., Cheng, H., Edwards, R.L., He, Y., Kong, X., An, Z., Wu, J., Kelly, M.J., Dykoski, C.A., Li, X., 2005. The Holocene Asian monsoon: links to solar changes and North Atlantic climate. Science 308, 854–857. https://doi.org/10.1126/science.1106296.
Wu, B., 2005. Weakening of Indian summer monsoon in recent decades. Adv. Atmos. Sci. 22, 21–29. https://doi.org/10.1007/BF02930866.
Wu, Y., Hu, C., Hu, Z., Liu, Y., Bräuning, A., 2023. Quantitative relative humidity reconstruction combining tree-ring with ice core oxygen isotope records. J. Hydrol. 617, 129084 https://doi.org/10.1016/j.jhydrol.2023.129084.
Xu, H., Song, Y., Goldsmith, Y., Lang, Y., 2019. Meridional ITCZ shifts modulate tropical/subtropical Asian monsoon rainfall. Sci. Bull. 64, 1737–1739. https://doi.org/10.1016/j.scib.2019.09.025.
Xue, J., Ning, L., Liu, Z., Qin, Y., Chen, K., Yan, M., Liu, J., Wang, L., Li, C., 2023. The combined influences of Solar Radiation and PDO on Precipitation over Eastern China during the last millennium. Clim. Dynam. 60, 1137–1150. https://doi.org/10.1007/s00382-022-06372-4.
Xue, L., Zhao, K., Cui, Y., Liang, Y., Yang, S., Wang, Y., 2020. Abrupt changes of East Asian summer monsoon over the past two millennia from stalagmite record in Luoshui Cave, Hubei Province. Quat. Sci. 40 (4), 973–984 (in Chinese).
Yang, B., Qin, C., Bräuning, A., Osborn, T.J., Trouet, V., Ljungqvist, F.C., Esper, J., Schneider, L., Grießinger, J., Büntgen, U., Rossi, S., Dong, G., Yan, M., Ning, L., Wang, J., Wang, X., Wang, S., Luterbacher, J., Cook, E.R., Stenseth, N.Chr, 2021. Long-term decrease in Asian monsoon rainfall and abrupt climate change events over the past 6,700 years. Proc. Natl. Acad. Sci. USA 118, e2102007118. https://doi.org/10.1073/pnas.2102007118.
Yang, X., Yang, H., Wang, B., Huang, L.-J., Shen, C.-C., Edwards, R.L., Cheng, H., 2019. Early-Holocene monsoon instability and climatic optimum recorded by Chinese stalagmites. Holocene 29, 1059–1067. https://doi.org/10.1177/0959683619831433.
Yin, J., Yuan, D., Li, H., Cheng, H., Li, T., Edwards, R.L., Lin, Y., Qin, J., Tang, W., Zhao, Z., Mii, H., 2014. Variation in the Asian Monsoon Intensity and Dry-Wet Condition since the Little Ice Age in Central China Revealed by an Aragonite Stalagmite. https://doi.org/10.5194/cpd-10-1305-2014.
Zhang, H., Ait Brahim, Y., Li, H., Zhao, J., Kathayat, G., Tian, Y., Baker, J., Wang, J., Zhang, F., Ning, Y., Edwards, R.L., Cheng, H., 2019. The asian summer monsoon: teleconnections and forcing mechanisms—a review from Chinese speleothem $\delta^{18}O$ records. Quaternary 2 (3), 26. https://doi.org/10.3390/quat2030026.
Zhang, H., Griffiths, M.L., Chiang, J.C.H., Kong, W., Wu, S., Atwood, A., Huang, J., Cheng, H., Ning, Y., Xie, S., 2018. East Asian hydroclimate modulated by the position of the westerlies during Termination I. Science 362, 580–583. https://doi.org/10.1126/science.aat9393.
Zhang, J., Liang, M., Li, T., Chen, C., Li, J., 2022. Asian-Australian monsoon evolution over the last millennium linked to ENSO in composite stalagmite $\delta^{18}O$ records. Quat. Sci. Rev. 281, 107420 https://doi.org/10.1016/j.quascirev.2022.107420.
Zhang, P., Cheng, H., Edwards, R.L., Chen, F., Wang, Y., Yang, X., Liu, Jian, Tan, M., Wang, X., Liu, Jinghua, An, C., Dai, Z., Zhou, J., Zhang, D., Jia, J., Jin, L., Johnson, K. R., 2008. A test of climate, sun, and culture relationships from an 1810-Year Chinese Cave Record. Science 322, 940–942. https://doi.org/10.1126/science.1163965.
Zhao, J., Cheng, H., Cao, J., Sinha, A., Dong, X., Pan, L., Pérez-Mejías, C., Zhang, H., Li, H., Wang, J., Wang, K., Cui, J., Yang, Y., 2023. Orchestrated decline of Asian summer monsoon and Atlantic meridional overturning circulation in global warming period. Innov. Geosci. 100011 https://doi.org/10.59717/j.xinn-geo.2023.100011.
Zhao, J., Cheng, H., Yang, Y., Liu, W., Zhang, H., Li, X., Li, H., Ait-Brahim, Y., Pérez-Mejías, C., Qu, X., 2021. Role of the summer monsoon variability in the collapse of the Ming Dynasty: evidences from speleothem records. Geophys. Res. Lett. 48, e2021GL093071 https://doi.org/10.1029/2021GL093071.
Zhao, K., Wang, Y., Edwards, R.L., Cheng, H., Kong, X., Liu, D., Shao, Q., Cui, Y., Huang, C., Ning, Y., Yang, X., 2020. Late Holocene monsoon precipitation changes in southern China and their linkage to Northern Hemisphere temperature. Quat. Sci. Rev. 232, 106191 https://doi.org/10.1016/j.quascirev.2020.106191.
Zhao, K., Wang, Y., Edwards, R.L., Cheng, H., Liu, D., Kong, X., 2015. A high-resolved record of the asian summer monsoon from Dongge cave, China for the past 1200 years. Quat. Sci. Rev. 122, 250–257. https://doi.org/10.1016/j.quascirev.2015.05.030.
Zheng, J., Wang, W.-C., Ge, Q., Man, Z., Zhang, P., 2006. Precipitation variability and extreme events in eastern China during the past 1500 years. Terr. Atmos. Ocean Sci. 17, 579. https://doi.org/10.3319/TAO.2006.17.3.579(A).
Zhou, T., Brönnimann, S., Griesser, T., Fischer, A.M., Zou, L., 2010. A reconstructed dynamic Indian monsoon index extended back to 1880. Clim. Dynam. 34, 573–585. https://doi.org/10.1007/s00382-009-0552-5.
Zhou, T., Gong, D., Li, J., Li, B., 2009. Detecting and understanding the multi-decadal variability of the east Asian summer monsoon recent progress and state of affairs. Meteorol. Z. 18, 455–467. https://doi.org/10.1127/0941-2948/2009/0396.